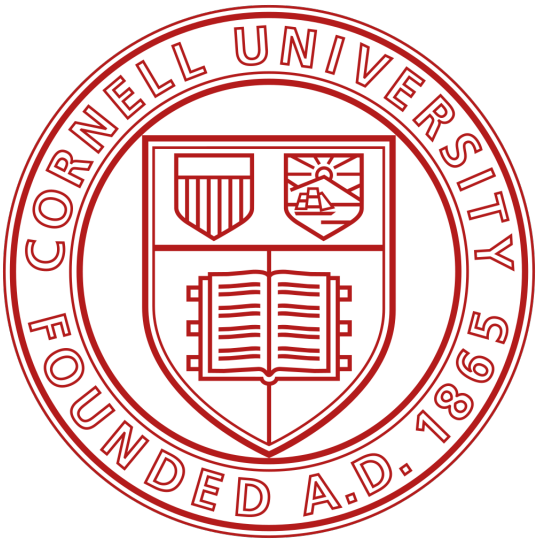

Cornell University

Department of Physics and Engineering

Ithaca, New York

Modeling Experimental Setup for In-Situ Thermal Mechanical Diffraction Applications

Author:
Joey Cavale

Advisors:
Chris Budrow
Tim Long
Kelly Nygren
Matt Miller

August 3, 2018

Abstract

The experimental setup for studying the thermal behaviors of a dual phase steel sample was modeled in Matlab to optimize the beam detector location. A parametric study was conducted on two metrics, percent overlap and total number of peaks, to help determine the best distance for the detector. After running through the simulation it was found that the optimal detector distances were 0.57, 0.65 and 0.66 meters with the best percentage overlap at 18.853% and a corresponding coverage of 14 peaks.

Introduction

The thermal behaviors and phase changes of various metals have been studied for many centuries. However, understanding what is happening deep inside the crystalline structures while the metal is experiencing these changes has yet to be discovered. High energy x-ray diffraction coupled with a thermal mechanical simulator will allow for the completion of in-depth, in-situ studies.

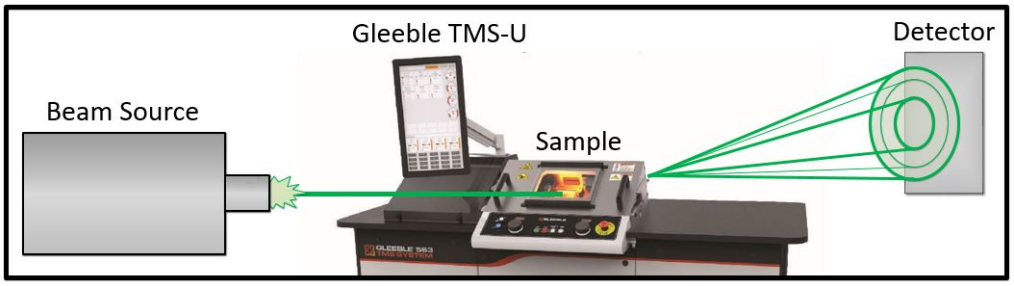

Figure 1: Experimental setup with Gleeble TMS-U.

Methods

MATLAB was used to simulate the experimental setup in order to optimize the position of the x-ray detector as seen in the figure above. The MATLAB script simulated a high energy, 61.332 keV, x-ray beam diffracting through a dual phase steel sample positioned inside of a Gleeble thermal mechanical simulator unit (TMS-U). As seen in Figure 2 below, the dual phase steel sample has separate phases that would also output two separate intensities.

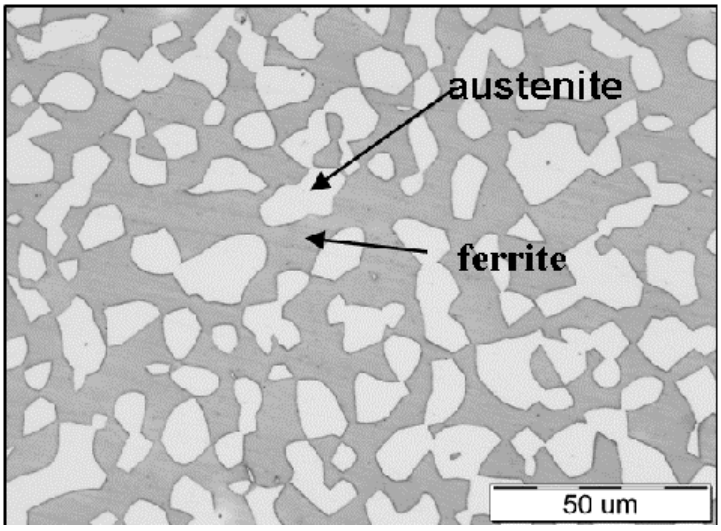

Figure 2: Dual phase austenite and ferrite steel sample. [1]

Analysis and Results

A Gaussian curve was used to model the diffracted x-ray beams which can be seen plotted below as beam intensity vs. the radius. The differing curves for each phase were plotted on top of one another and the percent of overlap was calculated, represented by the yellow shaded area in the figure to the right. This calculated overlap was coupled with the total number of peaks available to find the best detector distance.

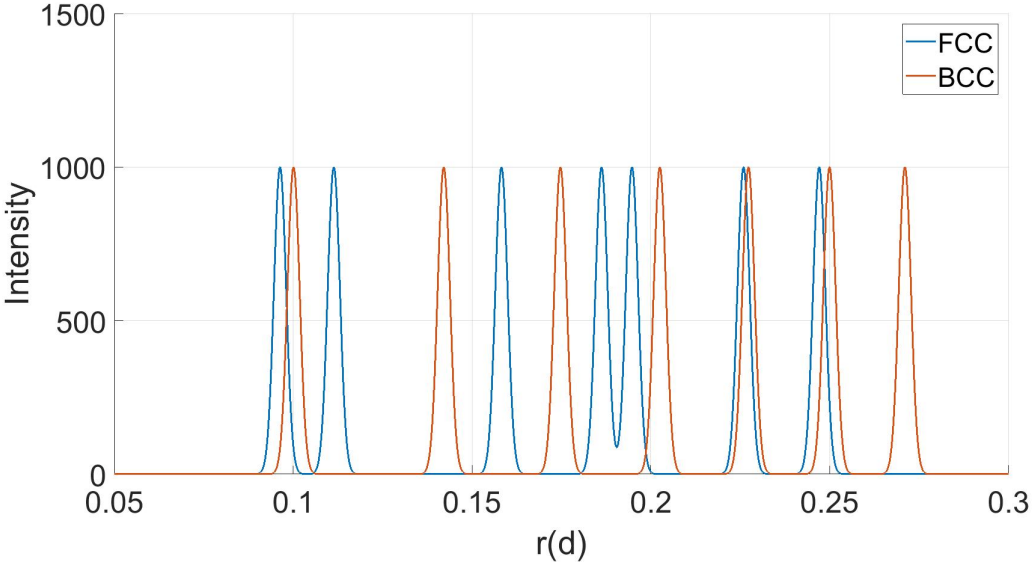

Figure 3: Plot showing austenite and ferrite phase intensities overlapping.

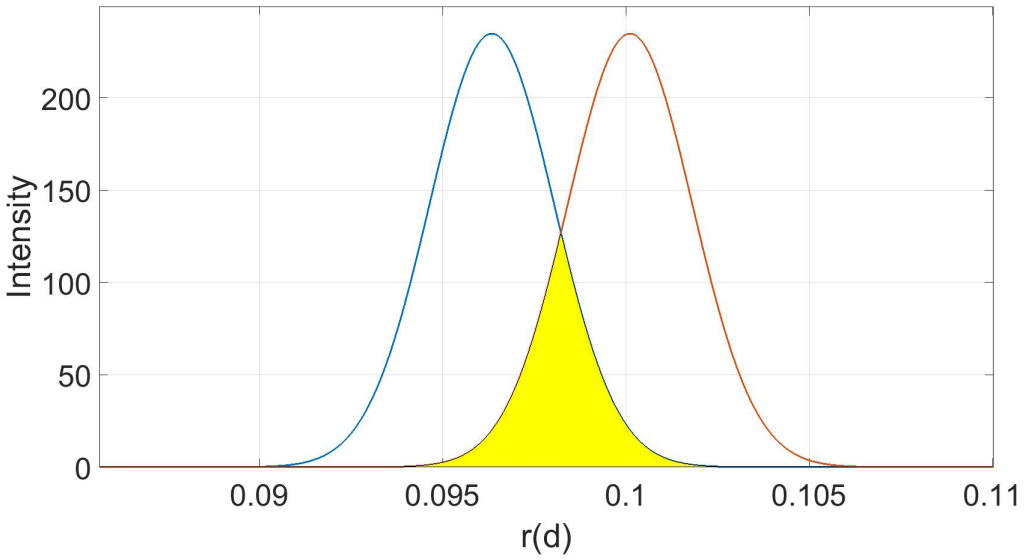

Figure 4: Gaussian overlap area and percentage calculation.

The simulation was conducted using a range of different detector distances and evaluated using defined metrics to help determine the best location. Shown below, a parametric study was conducted on two metrics and plotted versus the detector distance. Definitions of both metrics are listed below:

- The average percentage overlap was calculated to aid in determining the intensity peaks with the least amount of interference from the opposite phase.
- The number of peaks was a metric used to show the amount of data that could be captured with the detector located at the specified distance.

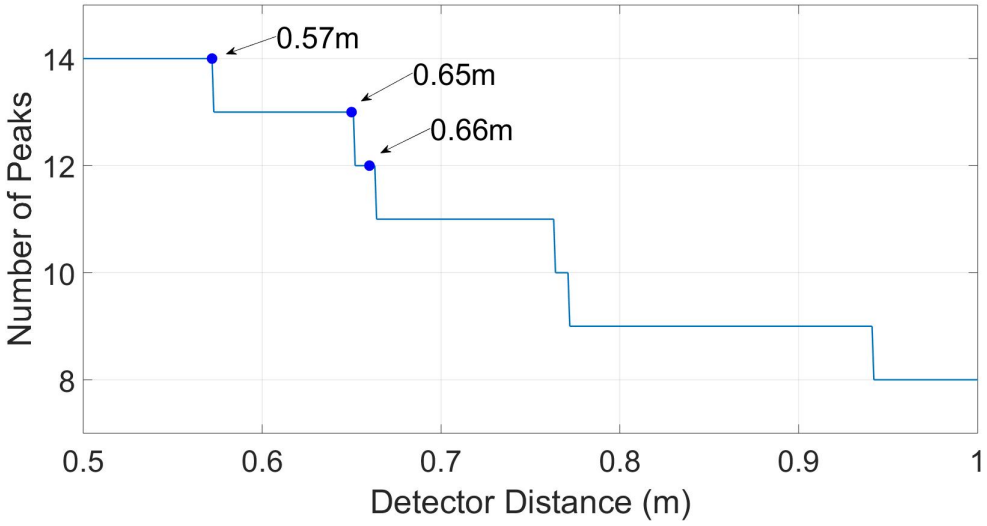

Figure 5: Gaussian overlap area and percentage calculation.

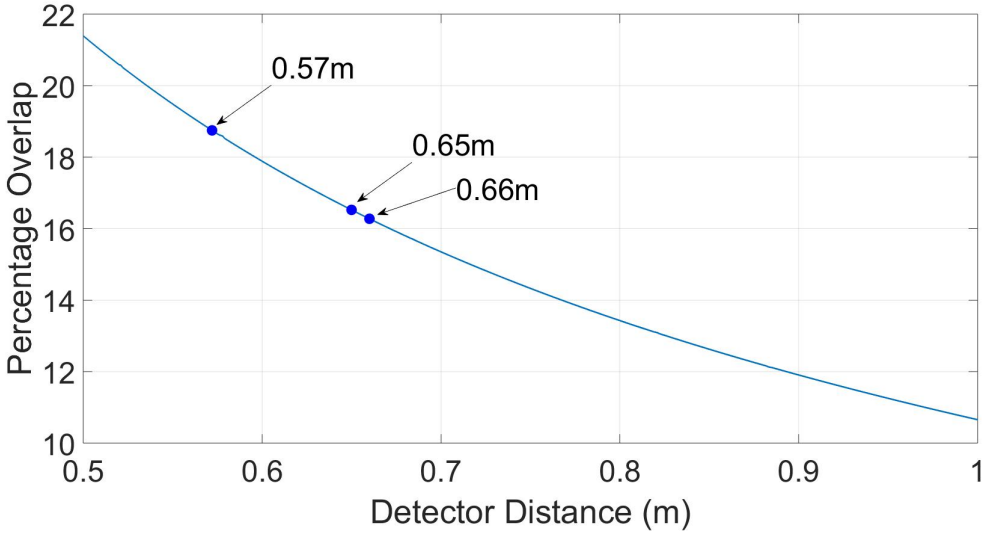

Figure 6: Gaussian overlap area and percentage calculation.

After the simulation was conducted, the optimum distances for the detector were determined to be 0.57m, 0.65m, and 0.66m. Holding the minimum percentage overlap as the highest importance, the detector distance of 0.57m was determined to be the best choice. The data acquired from the detector at 0.57m would be an overlap of 18.813% with a total peak coverage of 14 peaks.

Summary

Moving forward, this code provides an infrastructure for determining the optimum detector distance for future experiments in diffraction. This code can also be used as a quick analysis of peak overlap and detector coverage for data acquired later on. An optimized detector distance is integral to the next revolutionary step in understanding the fundamentals of materials science.

References

[1] The impact of deformation on structural changes of the duplex steel- Scientific Figure on ResearchGate. Available from: https://www.researchgate.net/Structure-of- the-X2CrNiMoN22-5-3-ferritic-austenitic- steel-after-solution-heat-treatment- fig1-40784245 [accessed 3 Aug, 2018]